Volume 1 | Number 1 | Jan 2013 | Pages 1–100

Nanoscale

www.rsc.org/nanoscale

ROYAL SOCIETY OF CHEMISTRY

www.rsc.org/nanoscale

Faradic redox active material of Cu_7S_4 nanowires with high conductance for flexible solid state supercapacitor

Muhammad Sufyan Javed[a,b], Shuge Dai[a], Mingjun Wang[a], Yi Xi[a], Qiang Lang[a], Donglin Guo[a], Chenguo Hu[a]*

[a] Department of Applied Physics, Chongqing University, Chongqing 400044, P. R. China

[b] Department of Physics, COMSATS Institute of Information Technology Lahore 54000, Pakistan

*Corresponding author. Tel: +86 23 65670880; Fax: +86 23 65678362

E-mail address: hucg@cqu.edu.cn (CG Hu)

Abstract

Exploration of high Faradic redox active materials with advantages of low cost and low toxicity has been attracted great attention for producing high energy storage supercapacitors. Here, the high Faradic redox active material of Cu_7S_4-NWs coated on the carbon fiber fabric (CFF) are directly used as a binder free electrode for high performance flexible solid state supercapacitor. The Cu_7S_4-NWs-CFF supercapacitor exhibits excellent electrochemical performance such as high specific capacitance of 400 F g^{-1} at the scan rate of 10 m Vs^{-1} and **high energy density of 35 Wh kg^{-1} at power density of 200 W kg^{-1}** with advantages of light weight, high flexibility and long term cycling stability by retaining 95 % after 5000 charge discharge cycles at constant current of 10 mA. The high Faradic redox activity and high conductance behavior of Cu_7S_4-NWs result in a high pseudocapacitive performance with relatively high specific energy and specific power. Such a new type of pseudocapacitive material of Cu_7S_4-NWs with low cost is very promising for actual application in supercapacitors.

Keywords: Copper sulfide, supercapacitor, ion-flow transportation, rigid cubiclattice, nanowires

1. Introduction

Environmental changes and declining of availability of fossil fuels require society to move towards sustainable and renewable energy resources with high efficiency and low to zero emissions. The major natural renewable resources are solar energy and wind energy but as these energy sources do not continuously supply energy so storage devices **are needed.** When we see towards electrical energy storage devices, batteries and electrochemical capacitors (ECs) also known supercapacitors (SCs) are forefront.[1-3] SC has high power density, long lifetime, quick charge rate and more environmental friendly compared with batteries. **These features make SCs promising energy storage devices in a broad range of applications, such as portable electronic devices, mobile phones, notebook computers, tablets, hybrid electric vehicles, military devices, industrial equipment and medical devices.[4-5]**

There are two kinds of supercapacitors based on charge storage mechanism electrochemical double layer supercapacitor (EDLC) and pseudocapacitor (PC). EDLCs are mostly based on **porous** carbon nanomaterials (grapheme, carbon nanotubes, and carbon aerogels) due to their high specific surface area and high electrical conductivity.[6] As electric charges physically stored on the surface of the porous carbon electrode limit the capacitance of the supercapacitor therefore high energy density supercapacitors require different technological solutions.[7] In contrast, pseudocapacitive type electrode materials can provide high energy density as compared to EDLC type electrodes. One strategy to increase the capacitance is related to Faradaic reactions based on pseudocapacitive behavior at the electrode/electrolyte interface. Pseudocapacitive materials are mainly based on metal oxides, hydroxides and conducting polymers which have much high specific capacitance as compared to EDLCs.[8] **The transition metal oxide and hydroxide such as RuO_2,[9] Co_3O_4,[10] NiO,[11] V_2O_5,[12] MnO_2[13] and Fe_3O_4[14] are considered as**

good candidate for PCs due to variety of reversible oxidation states for highly efficient redox charge transformation and high theoretical capacitance, but it is difficult to achieve high theoretical capacitance in practical applications because of poor electrical conductivity.[15] To enhance the electrical conductivity of them the considerable research have been focused on the hybrid composite nanostructures with conductive materials such as carbon nanotubes, graphene, conducting polymers[16] and sulfides.[17-18]

Recently nanostructured transition metal sulfides including that CoS,[19] MoS_2,[20] SnS,[21] NiS,[22] Ni_3S_2,[23] Bi_2S_3,[24] KCu_7S_4[25] and CuS[26] are used as electrode materials for supercapacitors due to both high specific capacitance and **low cost**. Usually, sulfides have larger crystal lattice distance and more complex valence states compared with oxides, which are favorable to electrolyte ion insertion and redox. It is known that copper sulfide (Cu_xS, x =1-2) forms a wide variety of non-stoichiometric and mixed phases, in which the location of Cu atoms in the close-packed S lattice are not well identified and their position changes as a function of x. Five of Cu_xS are known at least to be stable at room temperature: covellite (CuS) in the "sulfur-rich region"; and anilite ($Cu_{1.75}S$), digenite ($Cu_{1.8}S$), djurleite ($Cu_{1.95}S$), and chalcocite (Cu_2S) in the "copper-rich region".[27] **Among copper sulfide (Cu_xS, x =1-2), Cu_2S is considered to be a promising electrode material for lithium-ion batteries (LIBs) with a high theoretical capacity (282 mA hg^{-1}). However, one of the major problems hindering the application of Cu_2S in LIBs is its poor cycle stability, mainly caused by reactive polysulfide intermediates.[28]** Very recently, Han, et al. report that the Cu_2S/C composite displays good lithium-storage properties as a cathode material by gradually generating Cu_xS intermediate species.[29] Meanwhile, there are a few reports on CuS as an electrode material for supercapacitor due to good conductivity and valence change. Raj et al. prepare CuS nanoplates as an electrode material for supercapacitor

with maximum capacitance of 72.85 F g^{-1} with poor cyclic stability.[30] Hui Peng et.al reports hierarchical structures of CuS which exhibits the maximum specific capacitance of 597 F g^{-1} with 80 % capacitance retention after 1000 cycles.[31] Yu-Kuei Hsu et al. reports CuS nanowires as an electrode material for supercapacitor with maximum specific capacitance of 305 F g^{-1} with 87 % retention after 5000 cycles.[32] **As one of the nonstoichiometric copper sulfides Cu_7S_4 with Cu:S ratio of 1.75 is known as anilite.** To our best knowledge there is no report on Cu_7S_4 ($Cu_{1.75}S$) for supercapacitor electrodes. Based on theoretical calculation, it is found that under Cu-rich condition, the anilite $Cu_{1.75}S$ (Cu_7S_4) is the most stable structure in Cu_xS system.[33] whereas the S atoms in Cu_7S_4 form a rigid cubiclattice, providing a crystalline pathway for embedding of electrolyte ions, the copper ions around the S sublattice are superionic with "liquid-like" mobility.[34] Such specific ion-flow transportation behavior of copper ions around a crystalline sublattice of S in Cu_7S_4 might be important to improve pseudocapacitive performance.

The electrochemical performance of supercapacitor is also depends on the electrode material, **electrolyte** and current collector. The flexible power devices gain more attention to fulfill the needs of modern electronic devices. The flexible current collector, bendable, soft and elastic properties is the main requirements for making the flexible power devices, therefore soft current collectors such as papers, plastics, polymers and carbon textiles are extensively used to fabricate the flexible power devices.[35] **For easy portability, safety, flexibility and light weight a solid state electrolyte is much superior to liquid electrolyte.**

Herein we report the Cu_7S_4 with nanowire morphology, which was synthesized by a modified hydroxide mediated approach (M-HM) at 200 $^{\circ}$C. The Cu_7S_4-NWs coated on carbon fiber fabric (CFF) are directly used as a binder free electrode for high performance flexible solid state supercapacitor. The Cu_7S_4-NWs-CFF supercapacitor exhibits excellent electrochemical

performance with long term stability. Experimental results show that the large specific capacitance of 400 F g^{-1} at scan rate of 10 m Vs^{-1} and **high energy density of 35 Wh kg^{-1} at power density of 200 W kg^{-1}.** The good electrochemical stability has been demonstrated by 5000 charge-discharge cycles at constant current of 10 mA with 95 % retention of specific capacitance. The excellent electrochemical performance has been analyzed by crystal structure and conducting behavior indicating that is a result of specific ion-flow transportation behavior of copper ions around a crystalline sublattice of S in Cu_7S_4.

2. Experimental

2.1. Synthesis of Cu_7S_4 nanowires

Cu_7S_4-NWs were synthesized by a modified hydroxide mediated approach (M-HM) at low temperature in absence of any organic surfactant. As the melting point of pure sodium hydroxide is 323 °C, a small amount of water added into the sodium hydroxide can greatly reduce the melting temperature. In a typical experiment, 10 g of sodium hydroxide (NaOH), 0.198 g of cupper chloride ($CuCl_2$) and 0.24 g of sodium sulfide nonahydrate ($Na_2S.9H_2O$) were placed in a 25 mL Teflon vessel and 2 mL demonized water was added into Teflon vessel and then Teflon autoclave was put into furnace preheated to 200 °C for 24 hours. After reaction the autoclave was cooled down to room temperature naturally and then the black precipitate was washed many times with distilled water and absolute ethanol. The filtered product was put into oven for 24 hours at 60 °C for drying.

2.2. Preparation of supercapacitor

CFF (Shanghai Lishuo Composite Material Technology Company) was used to fabricate the supercapacitor. In the fabrication process, first CFF was cleaned with distilled water, acetone and

ethanol several times then it was cut into pieces of 5 cm × 2 cm and dry in oven. By using of vacuum pump deposit the Cu_7S_4-NWs on the CFF and dried at 60 ^{o}C in oven for 5 minutes. The mass loading of Cu_7S_4-NWs on CFF is approximately 1 mg cm^{-2}. The separator (Whatman 8 µm filter paper) and layer of LiCl-PVA gel as a solid electrolyte were sandwiched between two pieces of Cu_7S_4-NWs deposited CFFs. PVA-LiCl gel electrolyte was simply made as follow: 12.6 g of LiCl was mixed with 60 mL deionized water and then 6 g of PVA powder was added. The whole mixture was heated to 90 ^{o}C under vigorous stirring until the solution become clear. The CFF served as flexible current collector in the supercapacitor device. The schematic diagram of fabrication process of solid state flexible supercapacitor based on Cu_7S_4-NWs-CFF is shown in Figure 1. The bare CFF and Cu_7S_4-NWs coated on CFF are shown in Figure 2C and 2D respectively.

2.3. Structural and morphological Characterization

The chemical composition and crystal structure of the prepared sample was characterized by X-ray diffraction (PANalyticalX' Pert Powder). **The morphology of the prepared sample was investigated by scanning electron microscopy (FEI Nova 400 FEG-SEM). The specific surface area was measured by the multipoint Brunauer-Emmett-Teller (BET) method with Quadrasorb 2MP system.**

2.4. Electrochemical Measurements

The supercapacitor performance was checked by cyclic voltammetry (CV), galvanic charge-discharge cycles (GCD) in potential windows of -0.8 to 0.8 V and 0 to 0.8 V respectively. Different sweep rates (5, 10, 25, 50, 100, 150 and 200 m Vs^{-1}) were employed for evaluation the performance of supercapacitor. The GDC tests were measured at different current values ranging

from 5 to 15 mA. The electrochemical impedance spectroscopy (EIS) was carried out at 0.2 V

amplitude in a frequency range of 0.01-100 kHz at open circuit potential. These measurements

were conducted using an electrochemical workstation (CHI 760D). The specific capacitance

(Cs), energy density (ED), power density (PD) and columbic efficiency (η) of electrodes were

calculated according to the following equations.[10, 20, 25, 36]

$$C_S = \frac{1}{mv(V_f - V_i)} \int_{V_i}^{V_f} I \, dV \tag{1}$$

$$E = \frac{1}{2} CV^2 \times \left(\frac{1000}{3600}\right) \tag{2}$$

$$P = \frac{E}{t_d} = \frac{I\Delta V}{2m} \times 1000 \tag{3}$$

$$\eta \, (\%) = \frac{\Delta t_d}{\Delta t_c} \times 100 \tag{4}$$

Where C_s (F g^{-1}) is the specific capacitance; m (g) is the mass of active material on one electrode;

ΔV ($V_f - V_i$) is the potential window; v (Vs^{-1}) is the scan rate; I (A) is the applied current; E (Wh

kg^{-1}) is the energy density; P (W kg^{-1}) is the power density; Δt_d and Δt_c are discharging time and

charging time (s) and η **is the columbic efficiency of the solid state supercapacitor.**

3 Results and discussion

The synthesized Cu_7S_4-NWs are first characterized by X-ray diffraction (XRD) to identify its

crystallographic structure. Figure 2A shows the XRD pattern of Cu_7S_4-NWs where all diffraction

peaks could be indexed the **orthorhombic crystal** structure of Cu_7S_4 according to JCPDS No

33-0489; space group Pmna (62) with lattice parameters a = 7.905 Å, b = 7.822 Å and c =

11.07 Å. The strong and sharp diffraction peaks of XRD pattern suggest that the Cu_7S_4 product

is well crystallized. Figure 2B shows the crystal structure of the Cu_7S_4, from which we can see

that the S atoms in Cu_7S_4 form a rigid sublattice, and the copper ions around the S sublattice are

of ion-flow mobility.[34] **According to our previous report[37], carrier concentration, mobility**

and conductivity for the Cu_7S_4 film at room temperature are $3.05×10^{19}$ cm^{-3}, 5.46 cm^2 V^{-1} s^{-1},

10.88 S cm^{-1} respectively, indicating its high mobility and good conductivity which is higher

than CuS[38] (0.1 S cm^{-1} at room temperature) and CuS-polymer composite[39] (10 S cm^{-1} at

room temperature).

The morphology of prepared Cu_7S_4-NWs is shown in Figure 2E, which clearly indicates that the

Cu_7S_4 product has nanowire-like morphology with uniform size. **From high resolution image in**

Figure 2F, the average diameter of nanowires is about 100-150 nm. The small diameter, long

length and high specific area of nanowires will contributed to enhance the electrochemical

performance of the device. **The BET specific surface area of Cu_7S_4-NWs is about 34.23 m^2 g^{-1}**

, which is higher than that of the CuS nanotubes[40] (12 m^2 g^{-1}) and the CuS nanoflowers[41]

(18.8 m^2 g^{-1}).

The electrochemical performance of the Cu_7S_4-NWs-CFF solid state supercapacitor was checked

by cyclic voltammetry (CV) and galvanostatic charging-discharging (GDC). Figure 3A shows

the CV curves of Cu_7S_4-NWs-CFF supercapacitor. The CFF serves as a current collector and the

CV curve of CFF suggests that the substrate hardly contributes to the performance of

supercapacitor. The CV curves of Cu_7S_4-NWs-CFF at scan rates of 5-200 m Vs^{-1} in the potential

window of -0.8 to 0.8 V and at scan rates of 25-200 m Vs^{-1} in potential window of 0 to 0.8 V are

shown in Figure 3A and B, respectively. The shapes of CV curves clearly confirm the

pseudocapacitance behavior of Cu_7S_4-NWs, which is different from electrical double layer

capacitance behavior characterized by rectangular CV curves. The CV curves show a typically pseudocapacitive behavior of Cu_7S_4-NWs with Faradic redox peaks. The large oxidation and reduction peaks (redox peaks) appearing in the CV curves in the range of -0.6 to 0.6 V, which mainly attributed to the reversible insertion and extraction process of anions.

The high current response in the CV curves of Cu_7S_4-NWs-CFF also indicates the excellent charge storage ability and quick electrolyte ion accessibility of the electrode. This might be due to the high conductivity of Cu_7S_4-NWs and specific ion-flow transportation behavior of copper ions around a crystalline sublattice of S in Cu_7S_4 system. The specific capacitance C_s is calculated from CV curves according to the equation (1). The specific capacitances of 400, 245, 193, 121 and 109 F g^{-1} are calculated at the scan rate of 10, 25, 50, 100, and 150 m Vs^{-1} respectively. These values of specific capacitance are higher than that of CuS reported previously.[30, 32] The relationship between specific capacitance and scan rate is illustrated in Figure 3C. **The specific capacitance decrease from 400 to 193 F g^{-1} when scan rate increase from 10 to 50 m Vs^{-1}.** The specific capacitance is lower at the higher scan rates because the electrolyte-ions have not enough time to diffuse into the interior surface of the active material of the electrode, hence limited diffusion reduces the capacitance of the material. The oxidation and reduction peaks are nearly symmetric during the single scanning process and the peak current density is directly proportional to the square root of the scan rate as shown in Figure 3D. This behavior indicates that the redox reactions are reversible and controlled by the diffusion process at the electrode-electrolyte interface. **This kind of pseudocapacitance arises from the interaction/extraction of lithium ion in or on the surface of electrode, which can be represented by the following reactions.[28, 30, 42]**

$$Cu_7S_4 + zLi^+ + ze^- \rightarrow Li_zCu_7S_4$$

10

$$Li_z Cu_7 S_4 + zS \rightarrow Cu_7 S_4 + zLi_2 S$$
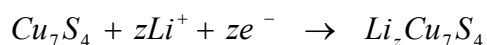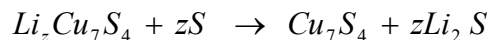
In these reactions the lithium ions interact with the Cu_7S_4 and occupied vacancy sites in the crystal lattice leading to the formation of complex ion of $Li_xCu_7S_4$. Finally $Li_xCu_7S_4$ reacts with sulfur ion and become Cu_7S_4 and Li_2S, and this product again contributes to the cyclic reactions of electrode. As ion-flow transportation behavior of copper ions could give the way to Li ions during the interaction/extraction process, the redox reactions would go easier. In addition, to find out the influence of electrolyte, the electrochemical performance of Cu_7S_4-NWs-CFF electrode in KOH electrolyte was measured. The CV curves in 1 M of KOH aqueous electrolyte at different voltage windows are shown in Figure S1, which indicate the unstable performance in accordance with previous report.[30]

Galvanostatic charge-discharge measurements are conducted at different current values ranging from 5 to 15 mA in the potential range of 0 to 0.8 V to further estimate the psudocapactive behavior of the Cu_7S_4-CFF supercapacitor and the results are shown in Figure 3E. The GDC curve is not straight lines and exhibits two different sections, a quick potential drop and slow potential drop, indicating that the faradic reaction is proceeding on. It is also clear from Figure 3E, the existence of plateaus at around 0.25 V in the charging curve suggests that the typical psudocapactive behavior of the electrode,[33] which is in good agreement of CV curves (Figure 3A). Furthermore the GCD curves show only a small voltage drop of 0.01 V at the start of the discharge curve, indicating a low internal resistance of the electrode material.

Electrochemical impedance spectroscopy (EIS) is powerful tool which give a wealth of information related internal resistances of electrodes-electrolyte system. The Cu_7S_4-NWs-CFF supercapacitor was further evaluated by (EIS) measurements. EIS of supercapacitor is measured

11

in the range of 0.01 to 100 kHz with potential amplitude of 0.2 V in order to evaluate the ionic resistance and kinetics of the electrodes. Nyquist plot of the supercapacitor is shown in Figure 3F, the lower and upper insets shows the enlarge semicircle in high frequency range and the equivalent circuit model to fit the EIS spectra using ZSimpWin impedance software, respectively. In the low frequency range the impedance characteristic is related to the diffusion of the ions between electrolyte and active material of the electrode. This behavior attributes the good capacitance performance of the device. In high frequency range the intercept at real axis characterizes ionic resistance of 3.54 Ω also known as equivalent series resistance (ESR) of the device, including the inherent resistance of material, contact resistance of electrode material and electrolyte. The low value of ESR indicates the good electrical conductivity between the electrode active material and current collector with low ionic resistance. The intercept with medium range of frequency is attributed to the charge transfer resistance (R_{ct}) due to faradic reactions on the surface of the active material.[20] Value of R_{ct} from inset of Figure 3F is 4.12 Ω. The low resistance of Cu_7S_4-NWs-CFF indicates the fast electron transfer between active Cu_7S_4-NWs material and current collector CFF. These low values also indicate consistent interfacial contact between Cu_7S_4-NWs and CFF. This is possibly due to the high specific surface area of Cu_7S_4-NWs which facilitates the effective exposure of active area and porous channels of CFF for ion flow transportation.

For practical applications lightweight, flexible, and portable electronic devices are gained more attention. In order to evaluate the potential as a flexible energy storage device the electrochemical performance is checked for the Cu_7S_4-NWs-CFF supercapacitor under various bending angles. Figure 4A shows the CV curves at different bending angles (flat, 45°, 180°, 360°) and according to these results there is no clear change in performance of the device. Figure

4B shows no change in the charge-discharge cycles under different bending angles even at 360° bending of the device. The capacitance ratio is almost equal to 1 **as is shown in Figure 4C, where the capacitance ratio is defined as the ratio between the capacitance of device at bent position to that at 0° or flat position**, demonstrating that the electrochemical performance of device is hardly affected by bending the device at different angles. Figure 4D shows the photographs of the Cu_7S_4-NWs-CFF supercapacitor bending in different angles.

In case of pseudocapacitors, degradation of the materials occurs after several hundred repeated redox reactions; therefore long lifetime is an important factor for the performance of pseudocapacitors. **Figure 5A shows there is slightly decrease in the performance of supercapacitor in the CV curves after and 5000th cycle in potential window of -0.8 to 0.8 V at constant scan rate of 100 m Vs^{-1}. The degradation might be due to the combination of the effect of delamination of active material due to ion insertion and due to the increase of internal resistance of the electrode material after long term cycling.** Figure 5B shows the long term charge-discharge curves at 100th and 5000th cycles at constant discharge current of 10 mA. After repeating 5000 charge-discharge cycles at constant discharge current of 10 mA the device loses only 5 % of its specific capacitance. A little difference in discharge time can be seen which is due to slight increase in the internal resistance of the electrode material. In order to further investigate the electrochemical stability, EIS is performed after completing 5000 charge-discharge cycles. The equivalent series resistance (ESR) of the supercapacitor slightly increases (0.07 Ω) after 5000 cycles as is shown in Figure 5C, which indicates that the electrode material and current collector is well attached throughout the working conditions of supercapacitor. The charge transfer resistance (R_{ct}) is evaluated approximately to be 4.12 Ω and 4.3 Ω before and after 5000 cycles, respectively.

The stability of the supercapacitor is also estimated by calculating the coulombic efficiency (η) at constant current of 10 mA using equation (4) and results are represented in Figure 5D. It can be seen that the columbic efficiency remains constant in the first 2000 cycles and then slight decreases till 3500 cycles and after that increases up to 5000 cycles with the maximum value of 95 %.

The long term cyclic performance of the Cu_7S_4-NWs-CFF supercapacitor is shown in Figure 6A. It can be observed that the specific capacitance slightly decreases till 2000 cycles, after that increasing slowly and attain the 95 % after completion of 5000 cycles. Mostly electrode materials for supercapacitors are fully active after several thousands of charge/discharge cycles. The reduction in capacitance means that electrode material is not full activated before 2000 cycles. The decay in specific capacitance compared with the maximum value after 5000 charge-discharge cycle test is only 5 %.

Energy density and power density are very important parameters for the evaluation of the performance of supercapacitors. The Ragone plot (energy density vs. power density) of Cu_7S_4-NWs-CFF supercapacitor is shown in Figure 6B. The energy density and power density are calculated using equations (2) and (3). **The highest energy density of 35 Wh kg^{-1} at power density of 200 W kg^{-1} is achieved, showing the potential application of the supercapacitor. The Cu_7S_4-NWs-CFF supercapacitor exhibits larger energy density and power density than that of the previous reported values for symmetric solid state supercapacitors, such as 1.7 Wh kg^{-1} at 8.3 W kg^{-1} for the V_2O_5/KCu_4Se_8,[36] 5 Wh kg^{-1} at 150 W kg^{-1} for the $Co_3V_2O_8$,[43] 7.25 Wh kg^{-1} at 186.5 W kg^{-1} for the sphere like MoS_2,[44] 23 Wh kg^{-1} at 284.2 W kg^{-1} for the nickel-cobalt layered double hydroxide nanowires[45]. The improved energy density and power density of the Cu_7S_4-NWs-CFF supercapacitor might be due to the following points:**

(1) Due to high conductivity and high surface area of Cu_7S_4-NWs. (2) The interfacial contact between electrolyte and active material is greatly improved due to the nanowire like morphology. (3) The one dimensional NWs are beneficial for insertion/extraction of Li^+ ions among them, which shorten the charge transfer path and also reduced the resistance between active material and electrolyte. (4) The Cu_7S_4-NWs were deposited on CFF without any press and binder which lead to the high performance of supercapacitor.

Figure 7A shows the GDC curves for single device, two devices and three devices connected in series at constant current of 10 mA. The single device can be charged to 1 V, two devices to 2 V and three devices to 3 V, demonstrating the practical application of Cu_7S_4-NWs-CFF supercapacitor. To demonstrate the potential use of Cu_7S_4-NWs-CFF supercapacitors, we connect three supercapacitors in series to light the light emitting diodes (LEDs) and the 6 red color LEDs can be effectively lit as is shown in Figure 7B.

4 Conclusions

In summary, highly conductive Cu_7S_4-NWs have been successfully synthesized by a modified hydroxide mediated approach at temperature of 200 ^{o}C. The carbon fiber fabric (CFF) is used as a current collector. The Cu_7S_4 structure has high conductivity due to the specific ion-flow transportation behavior of copper ions around a crystalline sublattice of S. The Cu_7S_4-NWs on CFF are directly served as a binder free electrode for high performance flexible solid state supercapacitor. The highly flexible Cu_7S_4-NWs-CFF supercapacitor shows the superior electrochemical performance. The electrochemical tests exhibit the maximum capacitance of 400 F g^{-1} at the scan rate of 10 m Vs^{-1} and high **energy density of 35 Wh kg^{-1} at power density of 200 W kg^{-1}**. It shows a good stability with 95 % retention of specific capacitance after 5000

charge-discharge cycles. Furthermore for practical applications three supercapacitors connected in series can light 6 red color LEDs (5 mm diameter, 2 V, 20 mA) effectively.

Acknowledgments

References

1. P. Simon, Y. Gogotsi, *Nat. Mater.*, 2008, 7, 845-854.

2. P. Yang, Y. Ding, Z. Lin, Z. Chen, Y. Li, P. Qiang, M. Ebrahimi, W. Mai, C. P. Wong, Z. L. Wang, *Nano lett.*, 2014, 14, 731-736.

3. P. Yang, W. Mai, *Nano Energy*, 2014, 8, 274-290.

4. Z. Zhang, Y. Zhang, K. Yang, K. Yi, Z. Zhou, A. Huang, K. Mai and X. Lu, J. Mater. Chem. A, 2015, 3, 1884-1889.

5. M. Yu, Y. Zhang, Y. Zeng, M. S. Balogun, K. Mai, Z. Zhang, X. Lu and Y. Tong, Adv. Mater., 2014, 26, 4724-4729.

6. P. Hao, Z. Zhao, J. Tian, H. Li, Y. Sang, G. Yu, H. Cai, H. Liu, C. Wong, A. Umar*, Nanoscale*, 2014, 6, 12120-12129.

7. P. Yang, Y. Chen, X. Yu, P. Qiang, K. Wang, X. Cai, S. Tan, P. Liu, J. Song, W. Mai, *Nano Energy,* 2014, 10, 108-116.

8. W. Zhou, X. Liu, Y. Sang, Z. Zhao, K. Zhou, H. Liu, S. Chen, *ACS Appl. Mater. Interfaces*, 2014, 6, 4578-4586.

9. A. Yu, V. Chabot and J. Zhang, *Electrochemical supercapacitors for energy storage and delivery: fundamentals and applications*, CRC Press, 2013.

10. R. Rakhi, W. Chen, D. Cha and H. Alshareef, *Nano letters*, 2012, **12**, 2559-2567.

11. G. Zhang, W. Li, K. Xie, F. Yu and H. Huang, *Adv. Funct. Mater.*, 2013, **23**, 3675-3681.

12. M.-H. Bai, L.-J. Bian, Y. Song and X.-X. Liu, *ACS appl. Mater. & interfaces*, 2014, **6**, 12656-12664.

13. M. Huang, X. L. Zhao, F. Li, L. L. Zhang and Y. X. Zhang, *J. Power Sources*, 2015, **277**, 36-43

14. S. Shivakumara, T. R. Penki and N. Munichandraiah, *ECS Elec. Lett.*, 2013, **2**, A60-A62.

15. J. Jiang, Y. Li, J. Liu, X. Huang, C. Yuan and X. W. D. Lou, *Adv. Mater.*, 2012, **24**, 5166-5180.

16. X. Sun, H. Sun, H. Li and H. Peng, *Adv. Mater.*, 2013, **25**, 5153-5176.

17. X. Rui, H. Tan, Q. Yan, *Nanoscale,* 2014*, 6*, 9889-9924.

18. M.-R. Gao, Y.-]F. Xu, J. Jiang and S.-H. Yu, *Chem. Soc. Reviews*, 2013, **42**, 2986-3017.

19 H. Wan, X. Ji, J. Jiang, J. Yu, L. Miao, L. Zhang, S. Bie, H. Chen, Y. Ruan, *J. Power Sources*, 2013, 243, 396-402.

20 M. S. Javed, S. Dai, M. Wang, D. Guo, L. Chen, X. Wang, C. Hu, Y. Xi, *J. Power Sources*, 2015, 285, 63-69.12

21 M. Jayalakshmi, M. M. Rao, B. Choudary, *Electrochem. Commun.*, 2004, 6, 1119-1122.

22 T. Zhu, Z. Wang, S. Ding, J. S. Chen, X. W. D. Lou, *RSC Adv.*, 2011, 1, 397-400.

23 C. Dai, P. Chien, J. Lin, S. Chou, W. Wu, P. Li, K. Wu, T. Lin, *ACS Appl. Mater. Interfaces*, 2013, 5, 12168-12174.

24 R. Mukkabla, M. Deepa, A. K. Srivastava, *Electrochim. Acta,* 2015, 164, 171-181.

25 S. Dai, Y. Xi, C. Hu, J. Liu, K. Zhang, X. Yue, L. Cheng, *J. Mater. Chem. A,* 2013, 1, 15530-15534.

26 L. Qian, X. Tian, L. Yang, J. Mao, H. Yuan, D. Xiao, *RSC Adv.*, 2013, 3, 1703-1708.

27. N. A. Yeryukov, A. G. Milekhin, L. L. Sveshnikova, T. A. Duda, L. D. Pokrovsky, A. K. Gutakovskii, S. A. Batsanov, E. E. Rodyakina, A. V. Latyshev and D. R. Zahn, *J. Phy. Chem. C*, 2014, **118**, 23409-23414.

28. R. Cai, J. Chen, J. Zhu, C. Xu, W. Zhang, C. Zhang, W. Shi, H. Tan, D. Yang and H. H. Hng, *J. Physical Chem. C*, 2012, 116, 12468-12474.

29. F. Han, W. Li, D. Li, A. Lu, *Chem. Electro. Chem.,* 2014, 1, 733-740.

30. C. J. Raj, B. C. Kim, W. Cho, W. Lee, Y. Seo, K. Yu, *J. Alloys Comp.,* 2014, 586, 191-196.

31. H. Peng, G. Ma, K. Sun, J. Mu, H. Wang, Z. Lei, *J. Mater. Chem. A*, 2014, 2, 3303-3307.

32. Y. Hsu, Y. Chen, Y. Lin, *Electrochim. Acta,* 2014, 139, 401-407.

33. Q. Xu, B. Huang, Y. Zhao, Y. Yan, R. Noufi, S. Wei, *Appl. Phys. Lett.,* 2012, 100, 061906.

34. H. L. Liu, X. Shi, F. F. Xu, L. L. Hang, W. Q. Zhang, L. D. Chen, Q. Li, C. Uher, T. Day and G. J. Snyder, *Nat. Mater.*, 2012, 11, 422.

35. D. Guo, Y. Luo, X. Yu, Q. Li and T. Wang, *Nano Energy*, 2014, **8**, 174-182.

36. K. Zhang, H. Chen, X. Wang, D. Guo, C. Hu, S. Wang, J. Sun, Q. Leng, *J. Power Sources,* 2014, 268, 522-532.

37. X. Li, C. Hu, X. Kang, Q. Len, Y. Xi, K. Zhang and H. Liu, *J. Mater. Chem. A*, 2013, 1, 13721-13726.

38. H. Grijalva, M. Inoue, S. Boggavarapu and P. Calvert, *J. Mater. Chem.*, 1996, 6, 1157-1160.

39. T. Yamamoto, E. Kubota, A. Taniguchi, K. Kubota and Y. Tominaga, *J. Mater. Sci. lett.*, 1986, 5, 132-134.

40. C. Wu, S.H. Yu, S. Chen, G. Liu and B. Liu, *J. Mater. Chem.*, 2006, **16**, 3326-3331

41. T.Y. Ding, M.S. Wang, S.P. Guo, G.-C. Guo and J.S. Huang, *Mater. Lett.*, 2008, **62**, 4529-4531.

42. B. Jache, B. Mogwitz, F. Klein and P. Adelhelm, *J. Power Sources*, 2014, 247, 703-711.

43. M.C. Liu, L.B. Kong, L. Kang, X. Li, F. C. Walsh, M. Xing, C. Lu, X.J. Ma and Y.C. Luo, *J. Mater.Chem. A*, 2014, **2**, 4919-4926.

44. K. Krishnamoorthy, G. K. Veerasubramani, S. Radhakrishnan and S. J. Kim, *Mater. Research Bulletin*, 2014, **50**, 499-502.

45. X. Wang, A. Sumboja, M. Lin, J. Yan and P. S. Lee, *Nanoscale*, 2012, **4**, 7266-7272.
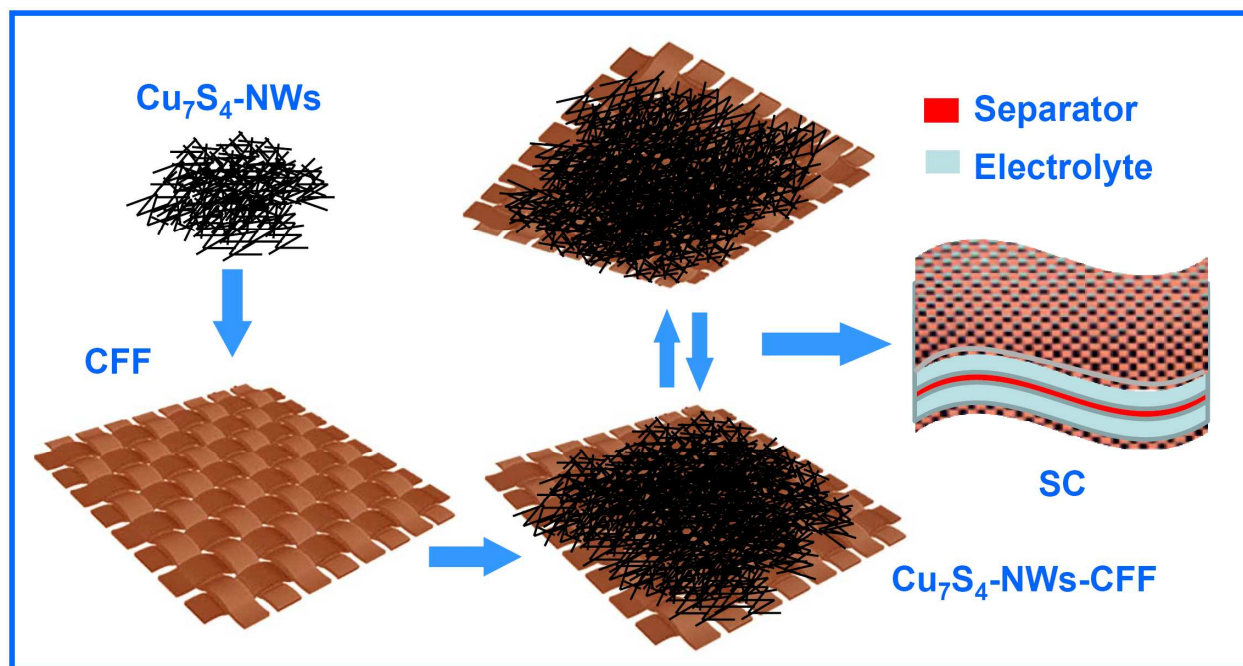
Figure 1. Preparation process of the Cu_7S_4-NWs-CFF supercapacitor.
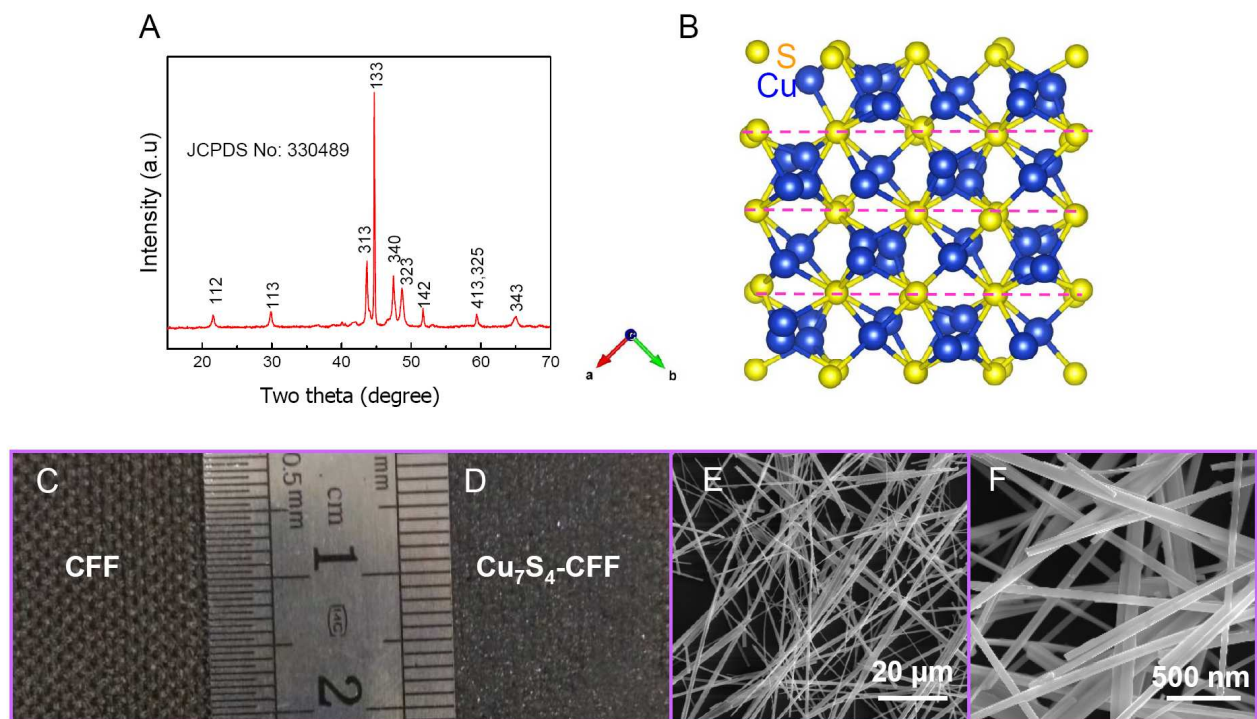
Figure 2. XRD pattern (A) and crystal structure of the synthesized Cu_7S_4-NWs (B), Photographs of CFF (C) and Cu_7S_4-NWs-CFF (D), and SEM images of the Cu_7S_4-NWs in low (E) and high (F) resolutions.
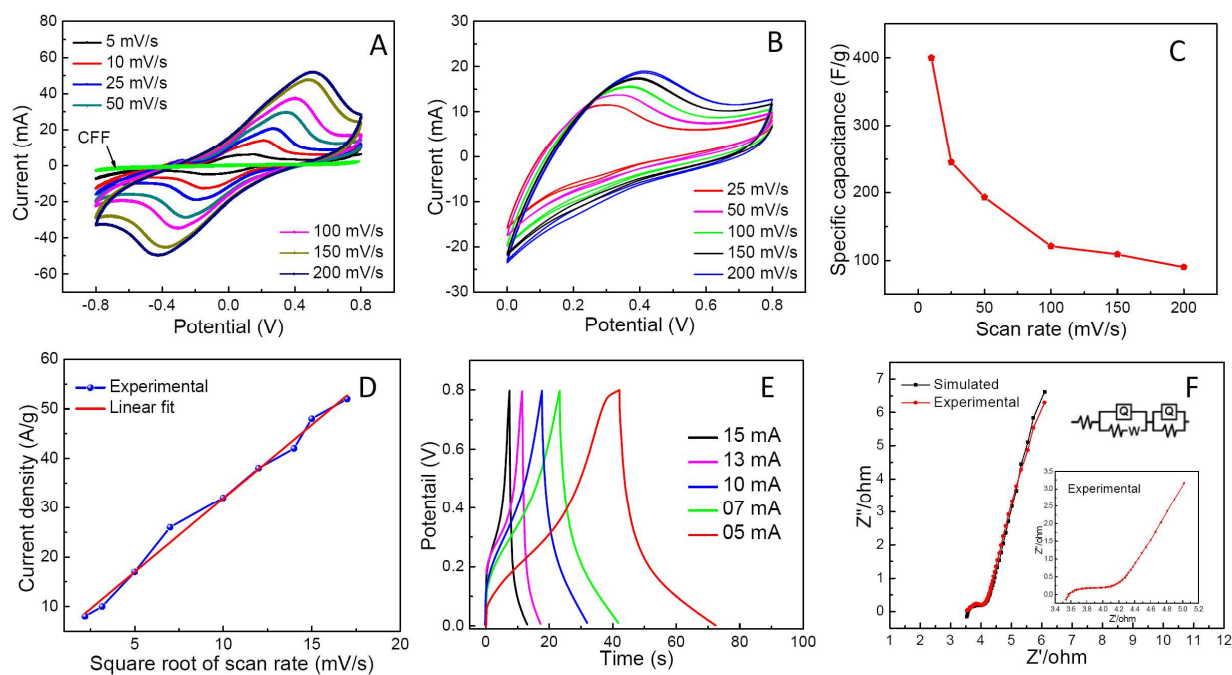
Figure 3. Electrochemical performances of the Cu_7S_4-NWs-CFF SC. (A) CV curves at different scan rates in potential window of -0.8-0.8 V (green curve for the CFF); (B) CV curves at different scan rates in potential window of 0-0.8 V; (C) Specific capacitance as a function of scan rate; (D) Current density vs. square root of scan rate, (E) GCD curves at the different current values; (F) Nyquist plot of impedance from 0.01 to 100 kHz, inset is the corresponding equivalent electrical circuit and enlarged semicircle.
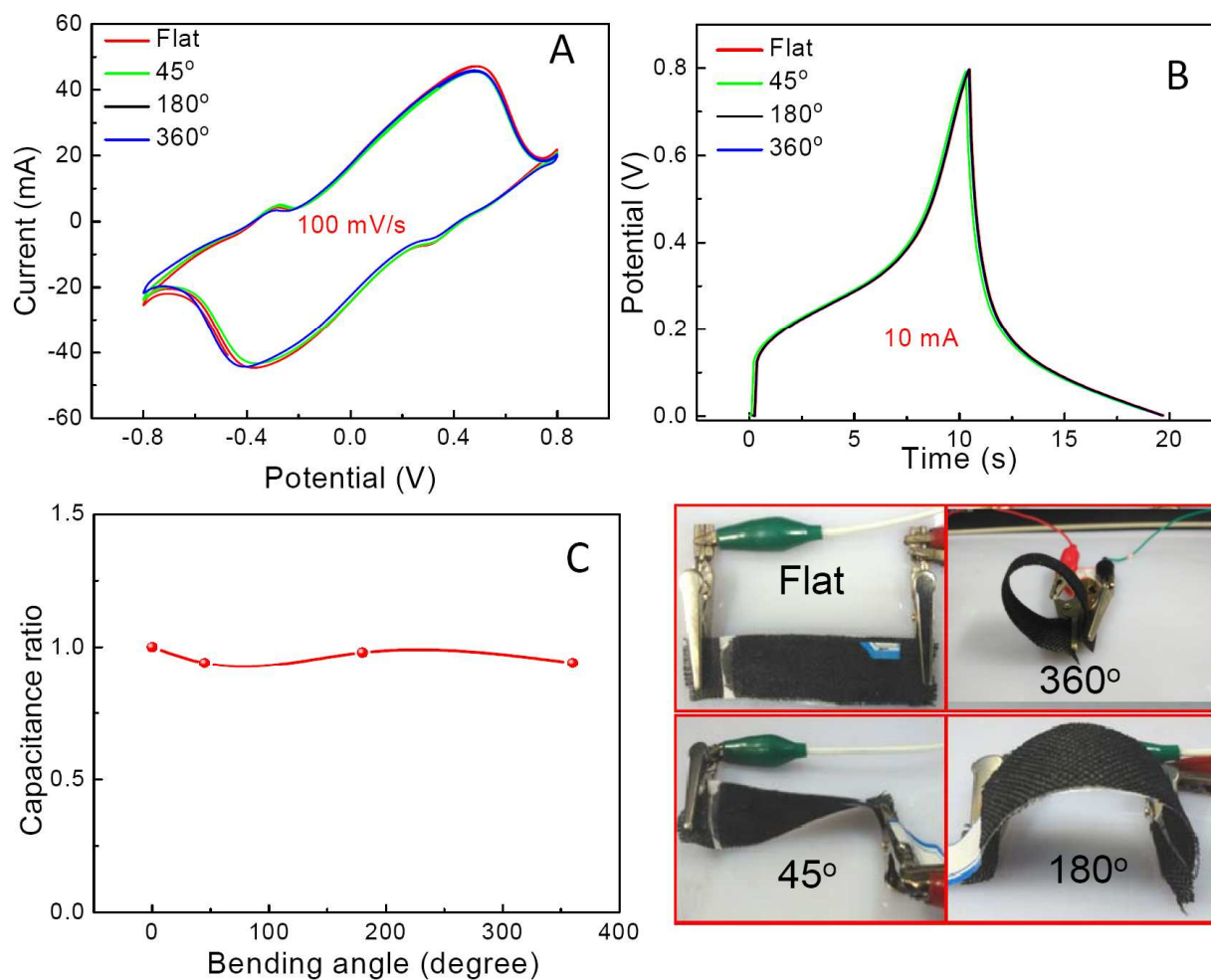
Figure 4. Performance of Cu_7S_4-NWs-CFF solid state SC at different bending angles. (A) CV curves at a scan rate of 100 mVs^{-1} and (B) charging-discharging curves taken at 10 mA, (C) bending angle vs. capacitance ratio, (D) Photographs of solid state supercapacitor bent in different angles showing the flexibility of the device.
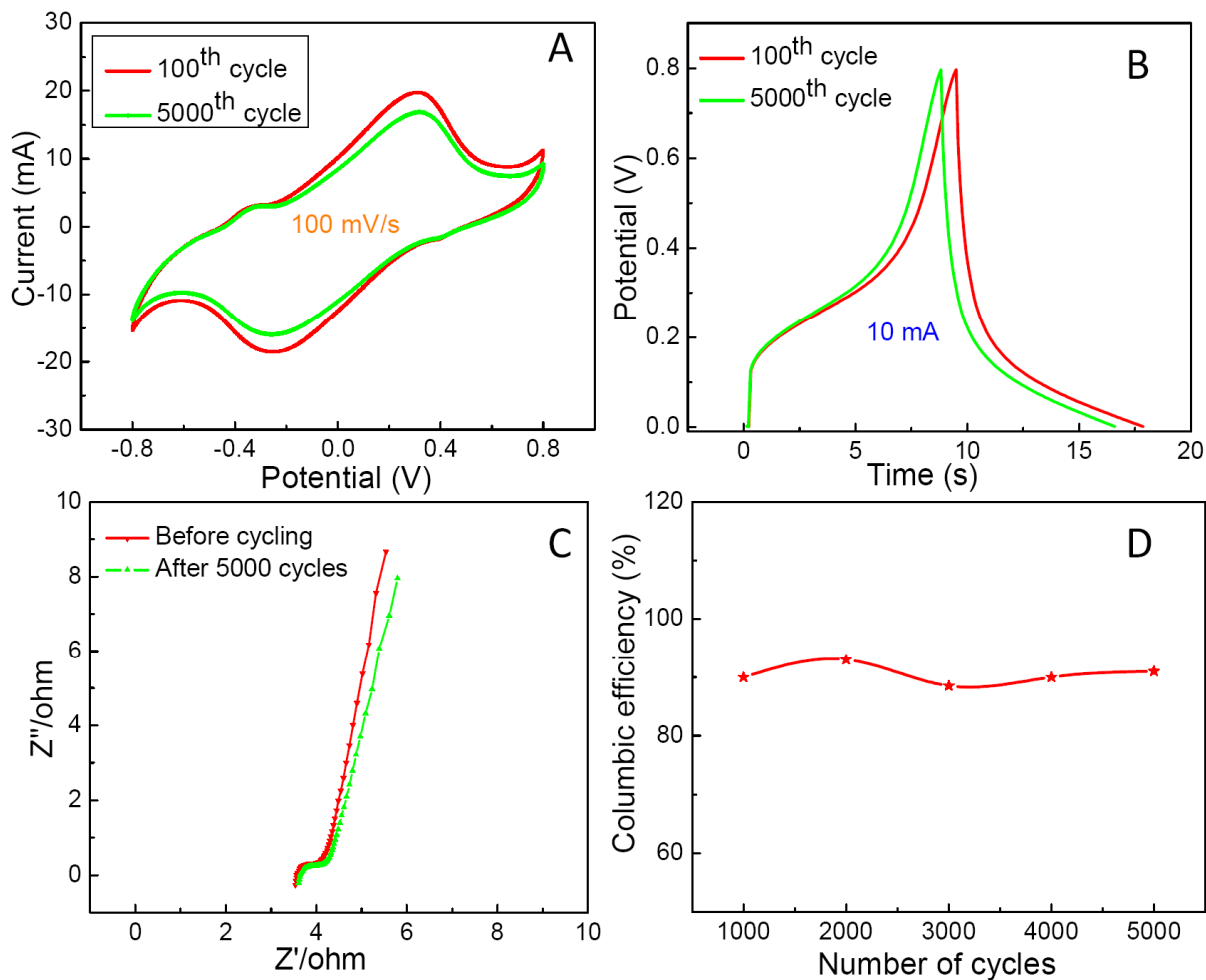
Figure 5. (A) CV curves of the Cu_7S_4-NWs-CFF SC for the 100th and 5000th cycles at scan rate of 100 mVs^{-1}, (B) Charging-discharging of the Cu_7S_4-NWs-CFF SC for the 100th and 5000th cycles, (C) EIS spectra before and after 5000 cycles, (D) Columbic efficiency of device vs. number of cycles.
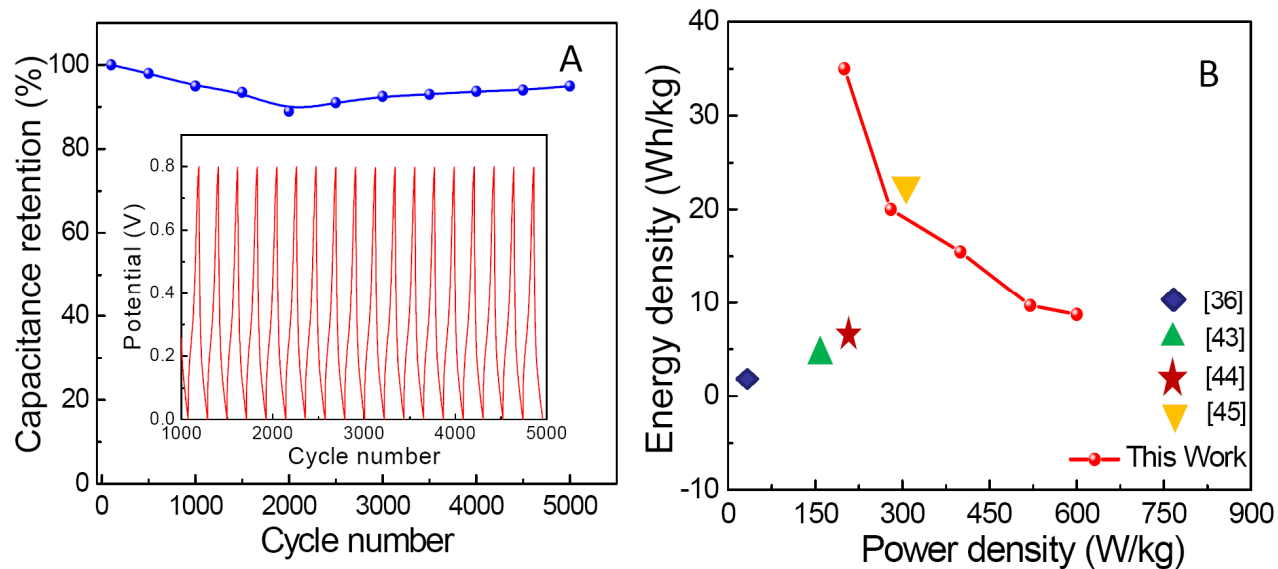
Figure 6. (A) Cyclic performance of the Cu$_7$S$_4$-NWs-CFF solid state SC at constant current of 10 mA. The inset shows its charge-discharge curves in potential window of 0 to 0.8 V at 10 mA. (B) Ragone plot (Energy density vs. Power density) of this supercapacitor and comparison with other reported data.
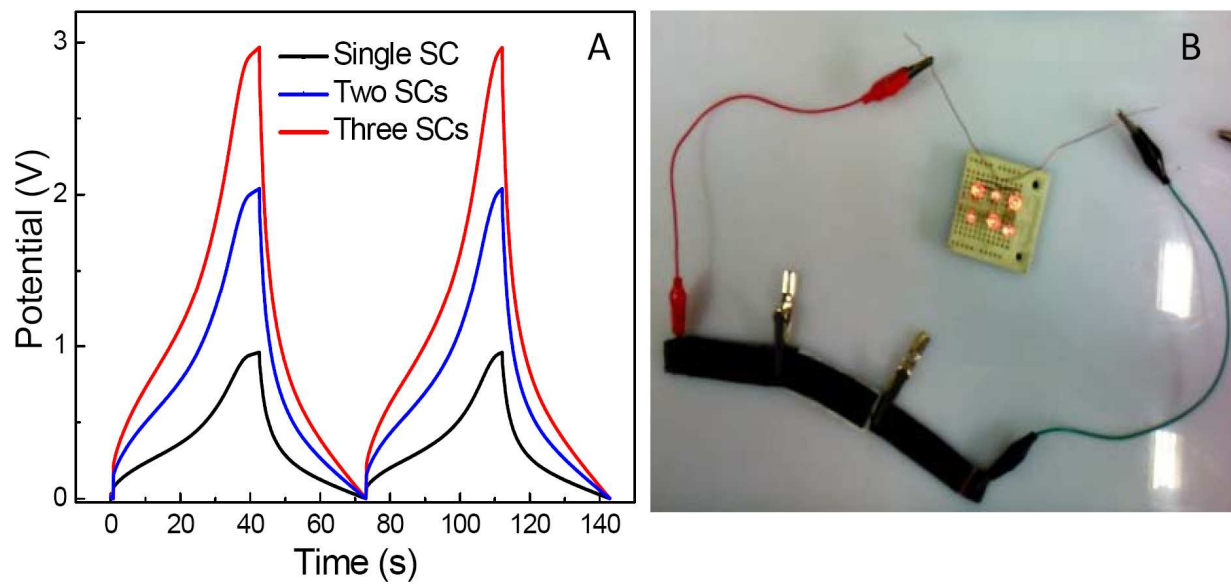
Figure 7. (A) Charging-discharging curves of Cu$_7$S$_4$-NWs-CFF SC at constant current of 10 mA fro Single, two and three devices in series respectively, (B) The digital photograph of 6 commercialized red color LEDs lit by three charged supercapacitors connected in series.